# Satellite-Based Estimation of Temporally Resolved Dust Radiative Forcing in Snow Cover

STEVEN D. MILLER AND FANG WANG

*Cooperative Institute for Research in the Atmosphere, Colorado State University, Fort Collins, Colorado*

ANN B. BURGESS

*Computer Science Department, University of Southern California, Los Angeles, California*

S. MCKENZIE SKILES

*Jet Propulsion Laboratory, California Institute of Technology, Pasadena, California*

MATTHEW ROGERS

*Cooperative Institute for Research in the Atmosphere, Colorado State University, Fort Collins, Colorado*

THOMAS H. PAINTER

*Jet Propulsion Laboratory, California Institute of Technology, Pasadena, California*

(Manuscript received 19 August 2015, in final form 26 April 2016)

ABSTRACT

Runoff from mountain snowpack is an important freshwater supply for many parts of the world. The deposition of aeolian dust on snow decreases snow albedo and increases the absorption of solar irradiance. This absorption accelerates melting, impacting the regional hydrological cycle in terms of timing and magnitude of runoff. The Moderate Resolution Imaging Spectroradiometer (MODIS) Dust Radiative Forcing in Snow (MODDRFS) satellite product allows estimation of the instantaneous (at time of satellite overpass) surface radiative forcing caused by dust. While such snapshots are useful, energy balance modeling requires temporally resolved radiative forcing to represent energy fluxes to the snowpack, as modulated primarily by varying cloud cover. Here, the instantaneous MODDRFS estimate is used as a tie point to calculate temporally resolved surface radiative forcing. Dust radiative forcing scenarios were considered for 1) clear-sky conditions and 2) all-sky conditions using satellite-based cloud observations. Comparisons against in situ stations in the Rocky Mountains show that accounting for the temporally resolved all-sky solar irradiance via satellite retrievals yields a more representative time series of dust radiative effects compared to the clear-sky assumption. The modeled impact of dust on enhanced snowmelt was found to be significant, accounting for nearly 50% of the total melt at the more contaminated station sites. The algorithm is applicable to regional basins worldwide, bearing relevance to both climate process research and the operational management of water resources.

## 1. Introduction

Mountain snowpack melting is a significant source of freshwater to arid and semiarid regions for more than a billion people worldwide (Bales et al. 2006), including ~40 million people in the United States and Mexico served by the upper Colorado River basin (UCRB; Painter et al. 2012b). The temporal behavior of runoff impacts agricultural activities, hydroelectric power generation, forest fire regimes, and other ecosystem processes (Westerling et al. 2006; Steltzer et al. 2009; Semmens and Ramage 2012). Thus, proper account and characterization of factors influencing the rate of snowmelt, such as deposition of light-absorbing impurities (e.g., soot and dust) upon snowpack, are of prime importance.

*Corresponding author address*: Steven D. Miller, Cooperative Institute for Research in the Atmosphere, Colorado State University, 1375 Campus Delivery, Fort Collins, CO 80523.
E-mail: steven.miller@colostate.edu

DOI: 10.1175/JHM-D-15-0150.1

Aeolian dust, transported long distances from the world's deserts, modulates the surface properties of snow and ice surfaces globally (Franzén et al. 1994; Wake and Mayewski 1994; Prospero 1999). The radiative forcing (RF) effects of dust on snow can be substantial. Early observational studies found that snow cover duration in the Colorado Rockies may be shortened by as much as 1 month because of dust effects (e.g., Jones 1913). More recent studies from detailed energy balance and radiation measurements show that snow cover duration in the UCRB is shortened by as much as 50 days because of mineral dust (Painter et al. 2007; Skiles et al. 2012). Bryant et al. (2013) show strong positive correlation between errors in operational streamflow predictions and the interannual variability of the direct effect of dust RF in snow (DRFS) in the UCRB.

There has been an observed trend toward increasing episodes of dust lofting in the western United States (Brahney et al. 2013), and it is suspected that human activity (e.g., domestic animal grazing, which can destabilize surface soils) has played a role (Painter et al. 2010). Dust loading in the Colorado Plateau has increased five- to sevenfold since Anglo settlement of the western United States in the mid-nineteenth century (Neff et al. 2008). Painter et al. (2010) compare periods before and after regional land-cover/land-use changes associated with human activities, finding that the peak runoff in the Colorado River basin is now 3 weeks earlier and the total annual runoff is 5% less.

The majority of dust events impacting the UCRB occur in the spring, when midlatitude cyclones loft dust from erodible surfaces over the desert southwest (Painter et al. 2012b; Wake and Mayewski 1994). Spring and summertime convection can also loft dust that is transported regionally (e.g., Miller et al. 2008; Corr et al. 2016). Such episodic events manifest as thin layers of contaminated snow residing between thicker layers of clean snowpack. Figure 1 shows the relatively dark appearance of dust-laden snow in contrast to clean snowpack in the San Juan Mountains of Colorado.

Whereas the physical basis for enhanced absorption of shortwave radiation is well established (Warren and Wiscombe 1980; Dozier 1989; Dozier and Painter 2004), translation of DRFS to late-season runoff behavior requires characterization of the spatial distribution and temporal evolution of these radiative properties. Nonuniformity of dust coverage and amount leads to a complex integrated downstream response that is best addressed through numerical modeling. Whereas point observations (e.g., streamflow gauges) provide high-temporal-resolution information, they do not provide the spatially resolved detail required for initializing models used for melting behavior and runoff prediction.

FIG. 1. Example of dust-laden snowpack in the San Juan Mountains of Colorado. (Photo courtesy of the Center for Snow and Avalanche Studies.)

Satellite remote sensing is well suited for monitoring DRFS over wide expanses of remote terrain. Optical-spectrum radiometers, such as the Moderate Resolution Imaging Spectroradiometer (MODIS) on the National Aeronautics and Space Administration's (NASA) *Terra* and *Aqua* satellites and the Visible Infrared Imaging Radiometer Suite (VIIRS) on the *Suomi National Polar-Orbiting Partnership* (*Suomi NPP*) satellite, provide spectral bands in the visible (VIS; e.g., 0.55 $\mu$m), near-infrared (NIR; e.g., 0.865 $\mu$m), and shortwave infrared (SWIR; e.g., 1.6 $\mu$m) that are essential to discriminating between snow cover and clouds in complex scenes (e.g., Hall et al. 1995). The observations also provide an ability to determine the radiometric properties of the snow cover. Since clean snow has high VIS reflectance and much lower SWIR reflectance, it is easily differentiated from other surfaces such as rock and vegetation. Even when snow is contaminated by dust, reducing its reflectance, the VIS/NIR ratio maintains an ability for unambiguous snow detection (Painter et al. 2012b).

The main limitation with MODIS and VIIRS is that they fly on low-Earth-orbiting (LEO) satellites, providing only 1–2 views over a given midlatitude region per day. While the impacts of dust can be determined at those specific times of day, the full radiative impacts vary with changing sun angle and the modulation of downwelling solar irradiance by clouds. This research expands the MODIS Dust Radiative Forcing in Snow (MODDRFS) algorithm developed by Painter et al. (2012a) from an instantaneous estimate of dust radiative forcing to a time-resolved and time-integrated estimate of total energy absorption over the course of a day. In so doing, the algorithm translates the results of MODDRFS into units of energy deposition, useful for

calculation of the actual snowmelt for a given day when coupled to an energy balance model.

The paper is outlined as follows. Section 2 provides motivation and the physical basis for this research. Section 3 describes the original MODDRFS algorithm and extends MODDRFS into the time-resolved domain for clear- and all-sky conditions. The all-sky version utilizes geostationary (GEO) satellite observations to account for the passage of cloud shadows over the dust-laden snowpack throughout the course of the day. Section 4 outlines a case study region used for proof-of-concept evaluation. Section 5 evaluates the algorithm for this case study, which includes in situ (point) validation data. Section 6 shows how the results of the time-resolved algorithm can be translated to equivalent snowmelt. These results are also compared against the case study in situ observations. Section 7 concludes the paper with a consideration of future sensor capabilities and associated research directions.

## 2. Physical basis

While clean snow cover exhibits the highest albedo of any naturally occurring surface on Earth, reflecting approximately 90% of the downward solar radiation incident upon it (Wiscombe and Warren 1980; Painter et al. 2012a), snow with light-absorbing impurities such as black carbon, mineral dust, or volcanic ash can exhibit a significantly lower albedo, reflecting less than 35% of the incident solar radiation. In the specific case of mineral dust (e.g., Fig. 1) the effect is strongest in the VIS wavelengths (Singh et al. 2010; Brandt et al. 2011). These mineral impurities increase the imaginary part of the bulk complex refractive index and thus increase the snow's absorption efficiency (Conway et al. 1996; Warren and Wiscombe 1980). This suppressed albedo (and hence, increased energy absorption by the snow) is considered the direct RF effect of dust on snow.

Increased absorption of sunlight, via the direct effect, can increase the rate of snow grain growth through more energetic metamorphism. As the effective grain size increases, there are further decreases in the albedo in the shortwave infrared (Hansen and Nazarenko 2004), leading to additional energy absorption. This process is known as the first feedback of the dust deposition and is captured implicitly by the remote sensing–inferred instantaneous DRFS. As melt progresses, meltwater percolates to deeper layers and the near-surface snow grain size begins to decrease again, dampening this positive system feedback (Painter et al. 2013). The direct effect and first feedback work in tandem to enable a second feedback, involving increased absorption of radiation by snow-free surfaces that have become exposed by accelerated snowmelt and loss. Here, we consider only the direct radiative impacts of dust on snow cover.

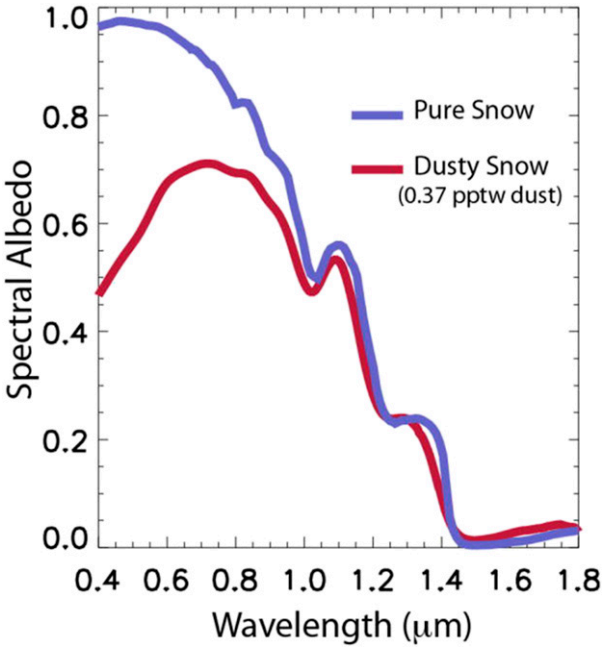


FIG. 2. Spectral albedo of clean snow (pure; modeled) and snow containing a surface dust concentration of 0.37 ppt by weight of snow water or mg $g^{-1}$ [measured; see Fig. 1 in Painter et al. (2012b)].

The direct effect of dust contamination on the spectral albedo of snow is illustrated in Fig. 2. The figure illustrates the preferential shortwave absorption imparted by hematite-bearing dust. Snow albedo drops significantly in the VIS through the NIR (from 0.95 to ~0.5 at 0.4 $\mu$m), whereas the differences are nearly negligible at wavelengths exceeding 1.0 $\mu$m. The dramatic reduction in surface albedo for dust-contaminated snow translates to a 4-factor increase in the absorption of shortwave radiation (Painter et al. 2007). Further, because light-absorbing impurities tend to remain near the surface as the snowpack melts (progressively lowering surface albedo) absorption of solar radiation increases stepwise over the snowmelt season (Conway et al. 1996; Painter et al. 2012a). The impacts are thus well observed by nadir-viewing remote sensing systems throughout the melting process when there is clear line of sight to the surface. These studies provide a solid physical basis for exploiting satellite observations to compute DRFS, detailed in the sections to follow.

## 3. Extending the MODDRFS algorithm to a time-resolved capability

The current work builds upon the MODDRFS algorithm of Painter et al. (2012a). MODDRFS computes a

daily gridded retrieval of dust RF ($W m^{-2}$) in snow from MODIS surface reflectance data (MOD09GA). These data are available from the NASA Jet Propulsion Laboratory (JPL) Snow Data System (http://snow.jpl.nasa.gov/). In this section, we briefly describe MODDRFS and extend this to the time-resolved domain.

### a. Overview of MODDRFS

First, MODDRFS discriminates snow pixels from nonsnow pixels using the normalized difference snow index (NDSI; Salomonson and Appel 2004). The optical grain radius (OGR) of snow is then determined for snow-covered pixels using the normalized difference grain size index (NDGSI; Painter et al. 2012a). NDGSI is identical in mathematical construct to NDSI, but uses MODIS band 2 (~0.86 $\mu$m) and band 5 (~1.240 $\mu$m), which provide stronger sensitivity to snow grain size. These bands have been quality controlled for detector striping in the MOD09GA surface reflectance product. NDGSI has a logarithmic relationship with OGR, as sensitivity to the hemispherical-directional reflectance factor (Schaepman-Strub et al. 2006) decreases with increasing OGR.

To conduct the MODDRFS retrieval, a clean snow spectrum is modeled for snow-covered pixels as a function of OGR and solar zenith angle using the discrete ordinates solution to the radiative transfer equation (DISORT; Stamnes et al. 1988). MODDRFS determines the difference between the spectral albedo of snow inferred from MODIS and the modeled clean snow spectral albedo of the equivalent OGR, where the difference is taken between 0.350 and 0.876 $\mu$m, assuming the divergence of dust-laden snow from clean snow reflectance does not occur at longer wavelengths (i.e., significantly less sensitivity to light-absorbing impurity properties and amount). Both measured and modeled spectra are splined to a spectral resolution of 0.01 $\mu$m. A clear-sky local spectral irradiance is estimated using the Santa Barbara DISORT Atmospheric Radiative Transfer (SBDART) model and the 3-arc-s Shuttle Radar Topography Mission (SRTM) digital elevation model (DEM). Last, to obtain surface RF by dust ($W m^{-2}$) the spectral difference between measured and modeled snow spectra is multiplied by the terrain-corrected irradiance.

Uncertainties in the MODDRFS retrieval are principally because of the coarse spatial and spectral resolution of the observations relative to scene variability. The multispectral observations provided by MODIS cannot capture the detailed spectral properties of light-absorbing impurities. The nominal footprint of MODIS at nadir (463 m) cannot describe the subpixel inhomogeneity of a snow-classified pixel, meaning that exposed soil/rock or vegetation will be misrepresented as light-absorbing impurities. Terrain relief and shadowing can introduce further complications to the scene reflectance. Other uncertainties include atmospheric correction (accounting for molecular scatter), sensor geolocation, variable sensor footprint size with sensor type and scan angle, and snow geographic/geomorphological properties. In light of these uncertainties, Painter et al. (2012a) estimate the root-mean-square and mean absolute errors for the MODDRFS retrieval as ~32 and ~25 $W m^{-2}$, respectively.

We leverage the MODDRFS algorithm described above as a basis for estimating the daily integrated RF. This estimate combines the instantaneous MODDRFS results with a time-resolved description of the downwelling solar irradiance. We develop the time-integrated MODDRFS in terms of both clear- and all-sky conditions—providing maximum potential and best estimate of actual DRFS impacts over the course of a given day.

### b. Clear-sky conditions

The baseline scenario of time-integrated dust RF assumes clear-sky conditions. This scenario can be regarded as a maximum possible daily value for dust RF, in contrast to a result that is modulated over time by the passage of cloud shadows. We begin with the instantaneous DRFS as estimated at satellite observation time $t$. This instantaneous (derived at observation time) quantity comes from the original MODDRFS algorithm (Painter et al. 2012a) and is computed as

$$\mathrm{DRFS}(t) = \int_{\lambda_1}^{\lambda_2} F_0(\lambda, t) \times D(\lambda, t)\, d\lambda. \qquad (1)$$

Here, $F_0(\lambda, t)$ is the incident surface-level solar irradiance at wavelength $\lambda$ and time $t$ and is calculated at each integration time over the course of the daylight hours. Variable $D(\lambda, t)$ is the reflectance difference between clean and dust-laden snow at wavelength $\lambda$ and time $t$. The wavelength lower limit $\lambda_1$ is 0.35 $\mu$m, the upper limit $\lambda_2$ is 0.85 $\mu$m, and the integration interval is 0.01 $\mu$m.

The incident solar irradiance at the surface is composed of direct and diffuse downwelling components:

$$F_0(\lambda, t) = F_{\mathrm{dir}_{\mathrm{local}}}(\lambda, t) + F_{\mathrm{diff}}(\lambda, t), \qquad (2)$$

where $F_{\mathrm{dir}_{\mathrm{local}}}$ is the direct terrain-adjusted component and $F_{\mathrm{diff}}$ is the diffuse sky component. For a given pixel, $F_0$ is obtained from a lookup table generated by the SBDART model (Ricchiazzi et al. 1998), stratified as a function of date, time, latitude, longitude, surface elevation, and terrain slope and aspect geometry. The SBDART table contains both the direct and diffuse spectral irradiance at a wavelength resolution of 0.01 $\mu$m

for a range of solar zenith angles and elevation bands. The lookup table is built upon midlatitude winter atmospheric profile assumptions, done for consistency with the one used in the current MODDRFS operational version. New lookup tables can be tailored to different regions and/or seasons.

Because the SBDART calculation assumes a horizontal surface, to obtain $F_{\mathrm{dir}_{\mathrm{local}}}$ the direct irradiance $F_{\mathrm{dir}}$ needs to be adjusted to account for the local terrain orientation. The local solar zenith angle $\theta_{s_{\mathrm{local}}}$ to the local terrain can be calculated using the following relationship:

$$\cos\theta_{s_{\mathrm{local}}} = \sin\theta_s \times \sin s \times \cos(\phi_s - \alpha) + \cos\theta_s \times \cos s, \quad (3)$$

where $\theta_s$ is the solar zenith angle, $\phi_s$ is the solar azimuth angle, $s$ is the terrain slope, and $\alpha$ is the terrain aspect. These slope and aspect data were taken from the 3-arc-second SRTM DEM data extracted over the study region. The downwelling direct solar irradiance at the surface is based on the slant path through the atmosphere (defined by $\cos\theta_s$). Using Eq. (3), we adjusted this direct irradiance to account for the local terrain orientation according to

$$F_{\mathrm{dir}_{\mathrm{local}}} = F_{\mathrm{dir}} \cos\theta_{s_{\mathrm{local}}} / \cos\theta_s. \quad (4)$$

By this construct, the direct beam at the surface is unchanged from its original value if the local terrain is oriented horizontally. Otherwise, it is enhanced/suppressed depending on the local terrain's orientation relative to the horizontal. The downwelling diffuse component was assumed to be independent of terrain orientation and was not modified in these calculations.

To compute the daily integrated RF, Eq. (1) must be convolved with the diurnal cycle of solar irradiance under the simplifying assumption of a constant snow grain size. The time integration from sunrise to sunset (i.e., daytime solar insolation) is given by

$$\text{daily integrated DRFS} = \int_{\text{sunrise}}^{\text{sunset}} \mathrm{DRFS}(t)\, dt. \quad (5)$$

While $D$ is fixed over the course of the integration, it can be updated daily by the instantaneous MODDRFS retrievals. Times of sunrise and sunset and the time-varying solar geometry were calculated as a function of geographic location, date, and time. The integration interval (time step) for implementing Eq. (5) in the current demonstrations was set to 6 min, but in practice this interval is fully configurable.

If we impose the assumption that the snow properties remain constant during the interval between daily MODIS updates, that is, the grain size of the melting snow does not change over the course and the day, then $D(\lambda, t) = D(\lambda)$ and Eq. (5) can be expanded as follows:

$$\text{daily integrated DRFS} = \int_{\text{sunrise}}^{\text{sunset}} \int_{\lambda_1}^{\lambda_2} [F_{\mathrm{dir}_{\mathrm{local}}}(\lambda, t) + F_{\mathrm{diff}}(\lambda, t)] \times D(\lambda)\, d\lambda\, dt. \quad (6)$$

This key assumption of $D$ invariance is a significant source of uncertainty to the current algorithm, but will improve with the application of this technique to next-generation GEO satellite observing systems that will have the ability to utilize the updated $D$ at every observation time.

### c. *All-sky conditions*

As mentioned above, clear-sky daily integrated DRFS represents the maximum possible forcing scenario for the melting potential of a dust-covered snow surface, because cloud attenuation is neglected. In reality, clouds can attenuate, reflect, and redistribute solar radiation between the direct and diffuse components. In most cases (but not all), incoming solar irradiance at the surface is reduced (ignoring higher-order, three-dimensional effects of diffuse sky augmentation by cloud-side illumination), thus decreasing temporally resolved dust RF in snow by the passage of cloud shadows (e.g., Zhu and Woodcock 2014; Crawford et al. 2013; Hutchison et al. 2009). Here, cloud observations are introduced to the analysis in an attempt to assess a more realistic time-integrated dust RF in snow. The temporal information is based on cloud observations from a GEO satellite, from which a time-varying solar irradiance field is estimated. This information is coupled with the MODDRFS result to provide a cloud-modulated solar irradiance component to Eq. (6).

Observations from the current-generation GOES-West were used to provide 30-min-resolution cloud imagery. These data helped to determine the evolving cloud cover and cloud optical properties for a given scene. The National Oceanic and Atmospheric Administration's (NOAA) National Environmental Satellite, Data, and Information Service (NESDIS) Clouds from the Advanced Very High Resolution Radiometer Extended (CLAVR-x; e.g., Stowe et al. 1999; Heidinger et al. 2014; Walther and Heidinger 2012) software calculates cloud mask and property retrievals. CLAVR-x is a project to derive atmospheric and surface properties based on roughly 25 years of NOAA's AVHRR operational LEO satellite constellation. This retrieval has been extended to

accommodate several other satellite instruments, including GEO observations from GOES. The common processing framework of CLAVR-x allows it to generate multiple products, including cloud, aerosol, surface, and radiometric, on the same grid.

The downwelling solar irradiance at the surface (direct, diffuse, and total) is computed using NOAA's Satellite Algorithm for Shortwave Radiation Budget (SASRAB; Pinker and Laszlo 1992) radiative transfer code. Based on a multistation validation study, Sengupta et al. (2015) determine the SASRAB RMSE for global horizontal irradiance (GHI) to be $\sim 104\,\mathrm{W\,m^{-2}}$ for all-sky conditions (with $\sim 50\,\mathrm{W\,m^{-2}}$ for clear-sky and $\sim 130\,\mathrm{W\,m^{-2}}$ for cloudy conditions). SASRAB that has been coupled to the CLAVR-x code provides surface irradiance on the common grid. These data are in turn enlisted as input to our time-resolved MODDRFS algorithm in the current study. Three-dimensional effects, such as enhanced diffuse-sky irradiance from the side-illumination of clouds, are not accounted for here. As such, the all-sky surface irradiance is typically less than or equal to the clear-sky spectra.

The all-sky DRFS was calculated from the CLAVR-x/SASRAB-retrieved quantities. Surface downwelling shortwave all-sky flux (i.e., $F_0$) and its diffuse component (i.e., $F_{\mathrm{diff}}$) are both calculated by SASRAB. The direct component is derived as the residual of the total and diffuse components, $F_{\mathrm{dir}} = F_0 - F_{\mathrm{diff}}$. Because $D(\lambda)$ values are only available for cloud-free pixels, integrated results can only be assessed at locations where there were clear-sky conditions at the time of the MODIS overpass. As such, cloud-covered pixels occurring at the time of the MODIS observations (as identified in the MOD09GA surface reflectance product, mapped to the common grid for calculations) were masked out and not evaluated for the time-integrated estimates.

It is important to note that the direct and diffuse component solar flux values calculated by SASRAB (i.e., $F$; $\mathrm{W\,m^{-2}}$) are defined as broadband quantities over wavelengths between 0.2 and 4.0 $\mu$m. The fraction of this irradiance over the wavelength range of 0.35 and 0.85 $\mu$m [the range of the $D(\lambda)$ retrieval from MODDRFS] was estimated as the ratio of solar flux from 0.35 to 0.85 $\mu$m to the broadband-integrated solar flux from 0.2 to 4.0 $\mu$m. For the ranges of the solar zenith angle and elevation for this particular case, a scaling factor of 0.65 was determined. The direct irradiance component of $F$ is corrected to the local topography using the terrain data and Eqs. (4) and (5).

Since $F$ is no longer a spectral quantity in the CLAVR-x/SASRAB-based all-sky calculations, we follow suit by computing a spectrally integrated version of $D$ as well. Equation (6) is thus rewritten as

$$\text{daily integrated DRFS} = \int_{\text{sunrise}}^{\text{sunset}} [F_{\text{dir}_{\text{local}}}(t) + F_{\text{diff}}(t)] \times D\, dt. \quad (7)$$

Evaluation of Eq. (7) requires that $D$ (from MODIS) and $F$ (from GOES) exist at the same spatial resolution. For our evaluation of the algorithm (results section), all pertinent variables were thus remapped to a common 0.05°-resolution grid. Based on the entire day's CLAVR-x cloud retrievals from GOES-West, Eq. (7) was used to calculate the daily integrated dust RF, accounting for the evolving cloud cover at 30-min intervals.

In summary, the daily MODDRFS retrievals provide information about the instantaneous $D$ values, and GOES retrievals based on CLAVR-x/SASRAB provide time-resolved downwelling surface irradiance information. Used together, the integrated dust RF in snow could be calculated over the full duration of daylight. The next section presents results on the time-integrated MODDRFS algorithm as applied to a representative case study from the UCRB.

## 4. Validation data

To evaluate the time-integrated MODDRFS algorithm, we selected a region of the Rocky Mountains within 36°–40°N, 109°–105°W. This region, which is a well-observed part of the UCRB, is also well known for the influences of light-absorbing impurities in snowpack, primarily from the prolific sources of mineral dust in the U.S. desert southwest. Figure 3 shows true color imagery (created from atmospherically corrected red, green, and blue MODIS bands to replicate the appearance of color photography) from *Terra* MODIS collected at 1755 UTC 21 May 2010 (Julian day 141). Readily noted in the true color imagery are the marked contrasts that existed between the dust-contaminated snowpack in the southern and western portions of the region (San Juan Mountains) and cleaner snowpack to the northeast.

To evaluate our algorithm, the temporally resolved clear- and all-sky RF values were compared against coincident in situ surface RF from the three instrumentation towers in the upper Colorado River basin, also labeled in Fig. 3. Two of the sites are located in the Senator Beck Basin Study Area (SBBSA) in the San Juan Mountains—an alpine site (37.906 88°N, 107.7289°W) and a subalpine site (37.906 91°N, 107.711 26°W). These are in fact the same sites that were used to validate the MODDRFS algorithm (Painter et al. 2012a). Here, we included an additional site, Grand Mesa Study Plot (GMSP), located 150 km to the north of SBBSA on the northern rim of Grand Mesa in west-central Colorado

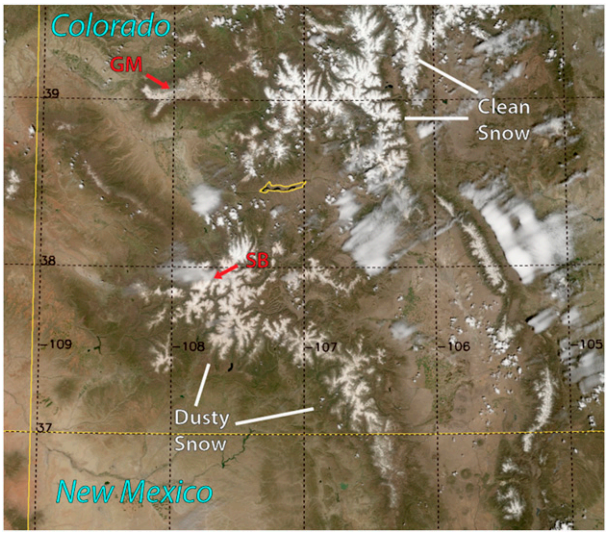


FIG. 3. True color imagery from *Terra* MODIS at 1755 UTC 21 May 2010 showing widespread regions of dust-contaminated snow on the San Juan Mountains of southwestern Colorado in contrast to cleaner snow cover to the northeast. Locations for the Grand Mesa (GM) and Senator Beck (SB) in situ sites considered in the analysis of satellite-derived dust radiative forcing on snow are indicated by red arrows.

(39.050 82°N, 108.061 42°W). Site photos of these three stations (collected on various dates) for various surface conditions are shown in Fig. 4. At each site, the validation towers are located in open fields to minimize the effects of shadowing from trees or terrain.

In addition to standard meteorological measurements (air temperature, wind speed, and relative humidity), the instrumentation towers measure incident and reflected broadband and NIR/SWIR solar radiation, with incident and reflected visible solar radiation component obtained by subtracting the NIR/SWIR component from the broad band (Painter et al. 2012a). The radiation measurements were used to determine RF due to dust from the relationships described in Painter et al. (2007), which calculates RF for two scenarios: a minimum RF case that accounts for the direct impact only (dust absorption) and a maximum RF case that accounts for both the direct and first indirect impact (grain growth). Since grain growth is not considered in the temporally resolved MODDRFS retrievals (discussed below), we used only the direct hourly RF from the towers for these comparisons:

$$\mathrm{RF}_{\mathrm{tower}} = E_{\mathrm{vis}}\Delta_{\mathrm{vis}}, \tag{8}$$

where $E_{\mathrm{vis}}$ is visible irradiance ($\mathrm{W\,m^{-2}}$; 0.305–0.780 $\mu$m) and $\Delta_{\mathrm{vis}} = 0.92 - \alpha_{\mathrm{vis}}$, with 0.92 representing a mean visible albedo for relatively clean snow at the SBBSA alpine site and $\alpha_{\mathrm{vis}}$ being the measured visible albedo.

## 5. Results

Figure 5 shows an evaluation of the reflectance difference between clean and dust-laden snow (i.e., $D$) for the same case study domain as Fig. 3. When combined with the downwelling solar irradiance, $D$ provides an estimate of the instantaneous dust RF [i.e., at the time of the MODIS overpass, via Eq. (1)]. Comparing Figs. 3 and 5, we see that higher values of $D$ correlate with areas of visually darker snow cover. These are the dust-laden


FIG. 4. Site photos of the instrumentation towers and surroundings at Senator Beck alpine (12 May 2009), Senator Beck subalpine (24 April 2013), and GMSP (6 May 2010).

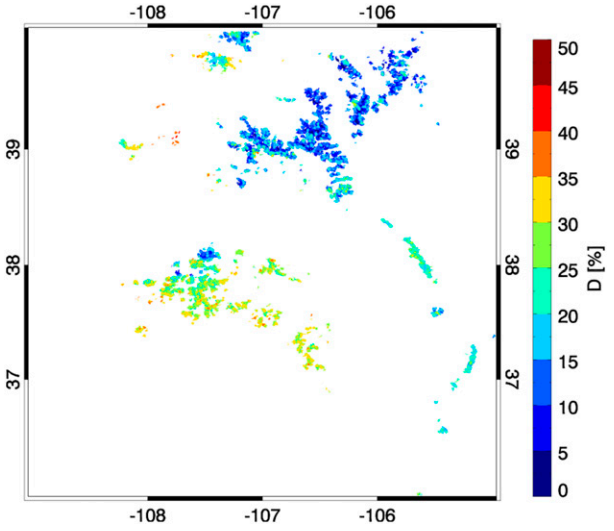


FIG. 5. MODIS-derived reflectance difference between clean and dust-laden snow, weighted by the solar-irradiance-weighted spectrum, over the case study region shown in Fig. 3 on 21 May 2010.

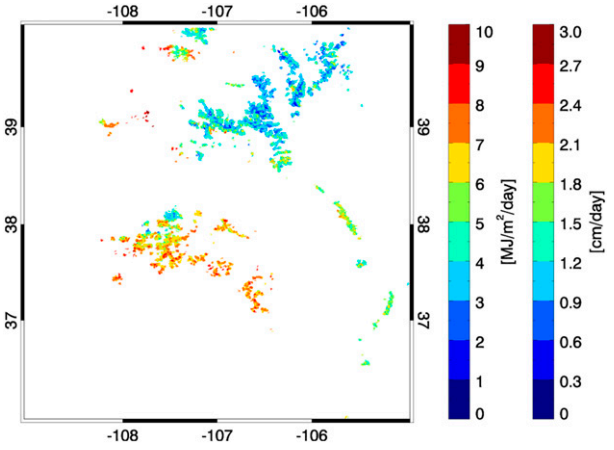


FIG. 6. Daily integrated dust RF in snow (MJ $m^{-2}$ $day^{-1}$) on 21 May 2010, assuming clear-sky conditions. The radiative forcing range, if averaged over a month, corresponds to ~1 m of melted SWE.

regions of the scene that will experience the most significant radiative impacts. In contrast, the relatively clean (bright white in Fig. 3) snow cover in the northeastern mountains corresponds to relatively lower values of $D$ in Fig. 5.

### a. *Instantaneous results*

In calculations done offline, absolute differences between our instantaneous dust RF at time of MODIS overpass and those of the operational MODDRFS were found to be from $-3$ to 1 W $m^{-2}$. These small differences, well within the uncertainty bounds of the algorithm, were due to slight differences between the SBDART irradiance lookup tables used in the current calculations and the operational algorithm lookup table. This close agreement provides a benchmark for evaluating the time-integrated versions of this algorithm.

### b. *Time-integrated results*

Figure 6 shows the daily integrated dust RF in snow for our case under the assumption of clear-sky conditions. These values are driven mostly by $D(\lambda)$. Figure 7a shows the corresponding daily integrated DRFS under all-sky conditions, rendered at 0.05° resolution. The gridded cloud mask is overlaid in grayscale to indicate those areas where $D$ values were not available at the time of the MODIS overpass (although these areas could contain snow pixels with or without dust deposition).

Compared with the clear-sky daily integrated DRFS, the all-sky values are significantly smaller because of the attenuation of solar energy by clouds. The difference between clear-sky (rebinned to 0.05°) and all-sky results is shown in Fig. 7b. Since all-sky contains both cloud and aerosol effects, the result is always lower than the clear-sky MODDRFS values, and hence these differences are positive definite. Owing to the enhanced absorption of dust-laden snow, the spatial variability is high, with its pattern following closely the distribution of $D$.

### c. *Comparisons against in situ RF observations*

Figure 8 shows the CLAVR-x/SASRAB (satellite estimated) direct and diffuse irradiance time series at the in situ sites. The SBBSA sites showed the effects of a broken cloud field in the morning, followed by a midday period of clear sky, and mostly overcast conditions in the afternoon. The GMSP site was generally clear in the morning, followed by more cloudiness in the afternoon. Both locations experienced clear-sky conditions around the time of the *Terra* satellite overpass at 1755 UTC (MODIS imagery shown in Fig. 3).

Figure 9 shows comparisons between the tower-derived (hourly averaged) and satellite-derived RF for the instrumented sites on 21 May 2010. Subhourly MODDRFS retrievals (blue points in Fig. 9) were averaged to match the hourly time step of in situ RF calculations. In situ daily mean (24 h) RF values, shown as horizontal lines in Fig. 9, were 35.7, 86.2, and 73.0 W $m^{-2}$ at the SBBSA alpine, SBBSA subalpine, and GMSP instrumentation sites, respectively. By inspection of the daily means of the relatively clean (Fig. 9, left; small RF) and dust-laden snow (Fig. 9, center and right; larger RF), we see that the spread between a clear-sky assumption (red line) and the all sky (reality; blue line) are substantially larger for the dust-laden snow cases.

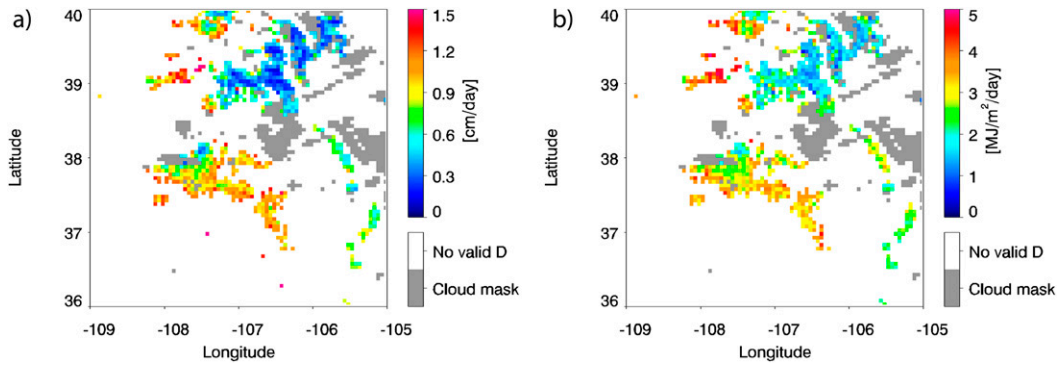


FIG. 7. Daily integrated dust RF in snow (MJ m$^{-2}$ day$^{-1}$) on 21 May 2010 for (a) all-sky conditions and (b) clear-sky (Fig. 6, rebinned) minus all-sky conditions.

While there was some hourly variation, the daily mean for in situ values (black horizontal lines) were found to be within the daily mean range for the clear- and all-sky conditions. At the SBBSA alpine and subalpine sites, the in situ RF was best matched to the clear-sky retrievals (daily means: 37.1 W m$^{-2}$ alpine and 100.3 W m$^{-2}$ subalpine). The all-sky retrieval indicates occasional suppressions, due to the passage of cloud shadows over the sites, which were not noted in the hourly-averaged tower data. At GMSP the daily mean in situ RF was only slightly higher than the all-sky retrieval (72.3 W m$^{-2}$), indicating that the satellite all-sky retrieval represented the behavior very well at this location.

## 6. Application to the modeling of snowmelt

To translate our radiative results to parameters relevant to river runoff, we used the all-sky RF retrievals as input to a point-based snow energy balance model. Our approach follows the methods of Painter et al. (2007) and Skiles et al. (2012). We enlisted the energy balance snowmelt model (SNOBAL; Marks et al. 1998), which has been shown to simulate snow cover depletion well—matching observed snow depletion date to within a day on average (Skiles et al. 2012; Skiles 2014). The model was provided with measured snow property inputs from the towers [i.e., a dust-laden snowpack, as performed in Skiles et al. (2012)]. We then removed the all-sky dust RF component from the measured net shortwave input and resimulated the snow cover evolution for a clean snowpack. The difference between the two scenarios represents the impacts of dust.

Hourly snow cover evolution over the course of 21 May 2010 was simulated with both the observed and simulated shortwave inputs. We then compared the modeled snow water equivalent (SWE; mm, from SNOBAL) for observed conditions to that of the

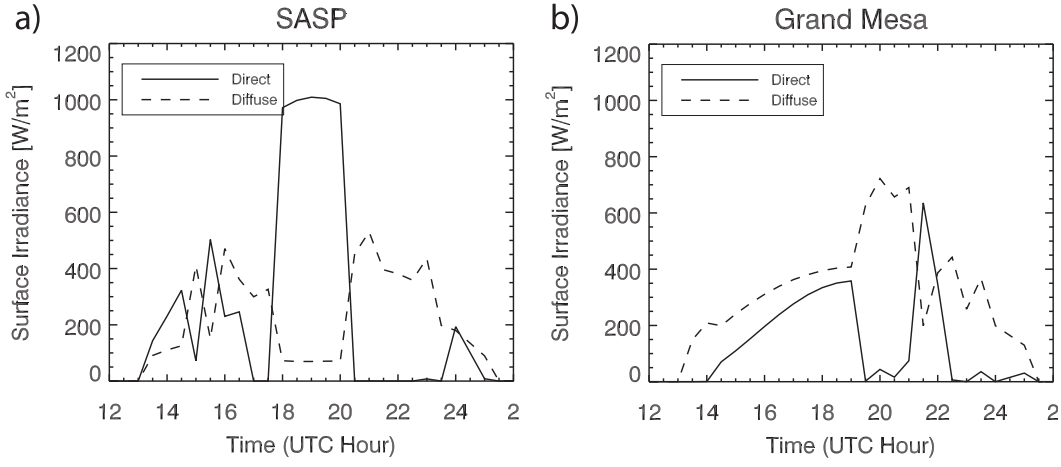


FIG. 8. Time series of satellite-estimated (CLAVR-x/SASRAB) downwelling shortwave surface direct and diffuse irradiance components on 21 May 2010 for in situ study areas at (a) Senator Beck and (b) Grand Mesa, as indicated in Fig. 3.

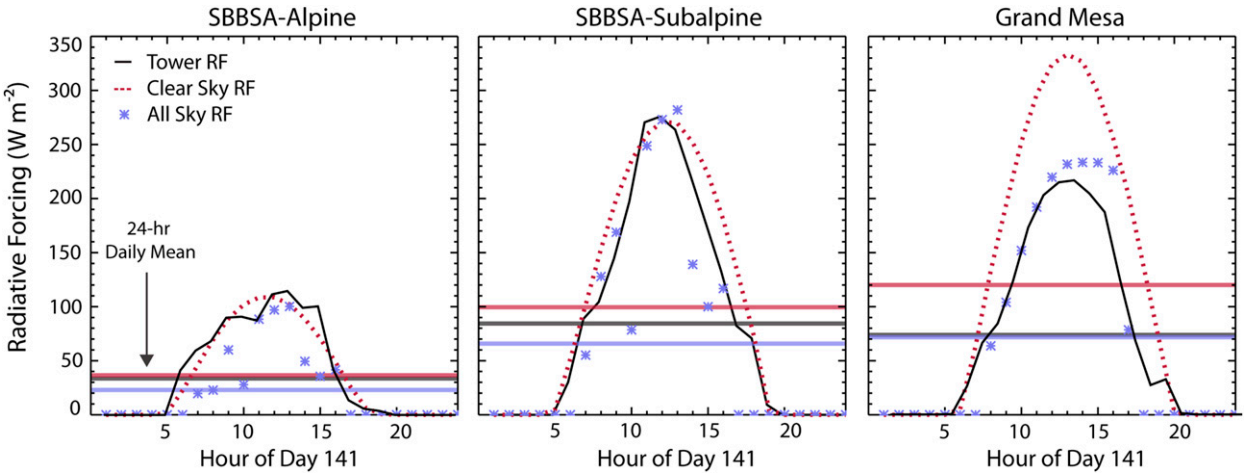


FIG. 9. Comparison of hourly radiative forcing from the clear- and all-sky retrievals and in situ radiative forcing at the three instrumentation towers on 21 May 2010. Solid horizontal lines represent 24-h daily means for each scenario.

clean-snow scenario. To examine the impacts of dust, we selected the difference in end-of-day SWE (ΔSWE) between the dust-laden (observed) and clean-snow scenarios.

Figure 10 shows results for the three instrumentation sites on 21 May 2010. At the SBBSA alpine site (the cleanest among the three sites and hence the lowest dust RF), the total SWE loss was estimated at 26.6 mm, with 20% (5.9 mm) of this melt due to the influences of dust absorption. At the SBBSA subalpine site, the total SWE reduction was 37.6 mm, with dust accounting for 46% (17.4 mm) of this melt. The impact was roughly proportional to the difference in RF between the SBBSA alpine and subalpine sites. At the GMSP site (Fig. 10, right), the total SWE reduction was 42.8 mm, with dust accounting for 45% (19.3 mm), similar in magnitude to dust forcing at the SBBSA subalpine site. The apparent SWE gain early on at GMSP is not due to precipitation, but rather is a by-product of snow density changing faster than snow depth.

Unfortunately, no SWE measurements were available on 21 May 2010. However, these measurements were available from the SBBSA subalpine site on 17 May (440 mm) and 24 May 2010 (302 mm). Using these straddling values and a simple linear assumption of SWE reduction, we estimated an SWE of 360 mm on 21 May. This estimate is within 3 mm of the modeled end-of-day SWE at the subalpine site (363 mm). The results, while local and

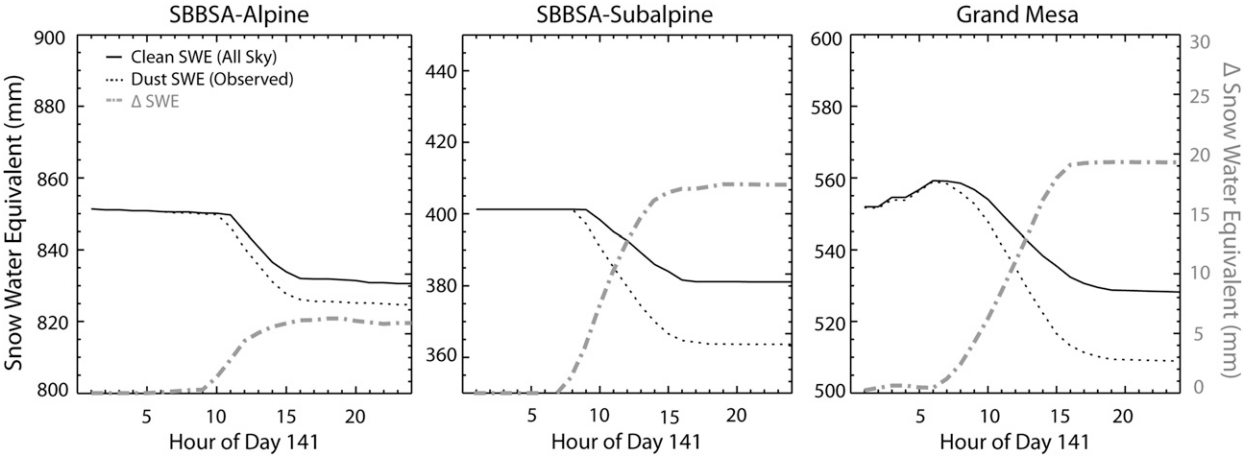


FIG. 10. Modeled SWE (left *y* axes; with different minima/maxima for each panel but each having an SWE range of 100 mm) and ΔSWE (right *y* axes; common for all panels) at the three instrumentation towers on 21 May 2010. The "dust SWE" scenario represents observed conditions and the "clean SWE" scenario has the all-sky dust radiative forcing removed to represent the evolution of snow cover in the absence of absorption by dust.

not comprehensive, are promising and indicate the potential for time-integrated MODDRFS estimates to provide useful information over larger spatial and longer temporal scales. Our study points to a need for more validation to demonstrate the fidelity of all-sky dust RF calculations over these scales.

## 7. Discussion and conclusions

A limitation of the current method is the assumed persistence of cloud coverage between satellite pass updates, which can introduce biases. Here, the significant influence of migratory cloud shadows (e.g., as might be expected in fair weather mountain cumulus field) are locked spatially to the 30-min update cycle of the current GOES. We anticipate that these sources of shadow persistence error in the current algorithm will be mitigated by more frequent updates from the next-generation GOES-R (5-min continental U.S. coverage down to 30-s mesoscale coverage; Schmit et al. 2005), slated for launch in late 2016. In addition, higher spatial resolution (0.5-km pixel size, or a 4-factor improvement over the current GOES) will improve the detail of cloud and shadow features.

The improved spectral suite of GOES-R (16 vs 5 bands on the current GOES) will afford improvements to the cloud mask and the associated shadow field and, most importantly, provide a direct measurement of time-resolved value of the spectral reflectance difference for clean versus dust-laden snow (analogous to what we must rely on MODIS for in the current work). Similar GEO capabilities managed by the Japanese, Korean, Chinese, and European meteorological satellite programs (initiated by the launch of Japan's *Himawari-8* satellite on 7 October 2014) are coming online in the next decade.

In a predictive sense, numerical weather prediction (NWP) models can be used to calculate the solar irradiance received at the surface under all weather conditions. The High-Resolution Rapid Refresh (HRRR; Weygandt et al. 2009), developed at NOAA's Earth System Research Laboratory (ESRL), represents the next generation of the Rapid Refresh (RAP) model, providing 3-km spatial resolution and 15-min updates out to 15-h forecast from hourly updated initialization times over the conterminous U.S. domain. It utilizes the coarser-resolution (13 km) RAP model, run operationally at the National Centers for Environmental Prediction (NCEP), as its boundary conditions.

The combination of satellite observations with high-resolution NWP models can provide both retrospective analyses and short-term forecasts of total (daily integrated) RF, and also the first time-resolved analysis of daily integrated dust RF in snow. The HRRR-derived forcing can be translated into predictions of enhanced snowmelt, so that the runoff timing and magnitude over a given watershed can be predicted with improved accuracy.

In summary, we have expanded the NASA/JPL MODDRFS retrieval to enable daily integrated estimates of dust RF in snow for both clear- and all-sky solar irradiance conditions. The daily integrated dust RF under clear-sky conditions represents a maximum RF potential, while the daily integrated dust RF under all-sky (i.e., including cloudy) conditions represents a more realistic value suitable for applications. It was shown that in both situations the forcing was mostly driven by the albedo difference due to dust deposition. For these dust-laden snow cover regions, the all-sky dust RF values were found to be significantly smaller than the clear-sky values. This is because of the suppression of downwelling solar irradiance by clouds, and particularly the direct beam component.

The in situ point analyses show general improvements to the satellite estimate of RF in comparison tower observations when the all-sky version of the algorithm is applied instead of a clear-sky assumption. This agreement was particularly notable at the Grand Mesa site, whose late-spring snowpack was visibly darker (Fig. 3) and exhibited commensurately large values of $D$. While the current analysis is by no means considered as comprehensive, it serves as a proof of concept for the algorithm and sets the stage for pursuing a more general and robust study (e.g., multiple case studies, regional and seasonal analysis) in work to follow.

As demonstrated by the SNOBAL simulations, the time-integrated RF information can be incorporated into a surface snow energy balance model to calculate the energy flux available for melt, thus providing a means for predicting the impact of dust on snowmelt (e.g., Marks and Dozier 1992). The estimated snowmelt could then serve as input to hydrological models for the improved prediction of river runoff behaviors. Such combined information holds potential value to National Weather Service River Forecast Centers and their downstream customers (water resource managers and hydrologic power providers).

*Acknowledgments.* This work was supported jointly by the Naval Research Laboratory through Contract N00173-10-C-2003, the Oceanographer of the Navy through the Program Executive Office C4I/PMW-120 under Program Element PE-0603207N, the Office of Naval Research through Contract N00014-16-1-2040 (Grant 11843919), and by NASA Project NNX10AO97G. We also thank Dr. Andrew Heidinger (NOAA/NESDIS)

and Dr. Andi Walter (University of Wisconsin–Madison) for providing the NOAA satellite processing packages used in this analysis.

## REFERENCES


Bales, R. C., N. P. Molotch, T. H. Painter, M. D. Dettinger, R. Rice, and J. Dozier, 2006: Mountain hydrology of the western United States. *Water Resour. Res.*, **42**, W08432, doi:10.1029/2005WR004387.

Brahney, J., A. P. Ballantyne, C. Sievers, and J. C. Neff, 2013: Increasing $Ca^{2+}$ deposition in the western US: The role of mineral aerosols. *Aeolian Res.*, **10**, 77–87, doi:10.1016/j.aeolia.2013.04.003.

Brandt, R. E., S. G. Warren, and A. D. Clarke, 2011: A controlled snowmaking experiment testing the relation between black carbon content and reduction of snow albedo. *J. Geophys. Res.*, **116**, D08109, doi:10.1029/2010JD015330.

Bryant, A. C., T. H. Painter, J. S. Deems, and S. M. Bender, 2013: Impact of dust radiative forcing in snow on accuracy of operational runoff prediction in the upper Colorado River basin. *Geophys. Res. Lett.*, **40**, 3945–3949, doi:10.1002/grl.50773.

Conway, H., A. Gades, and C. F. Raymond, 1996: Albedo of dirty snow during conditions of melt. *Water Resour. Res.*, **32**, 1713–1718, doi:10.1029/96WR00712.

Corr, C. A., and Coauthors, 2016: Observational evidence for the convective transport of dust over the central United States. *J. Geophys. Res. Atmos.*, **121**, 1306–1319, doi:10.1002/2015JD023789.

Crawford, C. J., S. M. Manson, M. E. Bauer, and D. K. Hall, 2013: Multitemporal snow cover mapping in mountainous terrain for Landsat climate data record development. *Remote Sens. Environ.*, **135**, 224–233, doi:10.1016/j.rse.2013.04.004.

Dozier, J., 1989: Spectral signature of alpine snow cover from the Landsat Thematic Mapper. *Remote Sens. Environ.*, **28**, 9–22, doi:10.1016/0034-4257(89)90101-6.

——, and T. H. Painter, 2004: Multispectral and hyperspectral remote sensing of alpine snow properties. *Annu. Rev. Earth Planet. Sci.*, **32**, 465–494, doi:10.1146/annurev.earth.32.101802.120404.

Franzén, L. G., J. O. Mattsson, U. Mårtensson, T. Nihlén, and A. Rapp, 1994: Yellow snow over the Alps and Subarctic from dust storm in Africa, March, 1991. *Ambio*, **23**, 233–235.

Hall, D. K., G. A. Riggs, and V. V. Salomonson, 1995: Development of methods for mapping global snow cover using Moderate Resolution Imaging Spectroradiometer data. *Remote Sens. Environ.*, **54**, 127–140, doi:10.1016/0034-4257(95)00137-P.

Hansen, J., and L. Nazarenko, 2004: Soot climate forcing via snow and ice albedos. *Proc. Natl. Acad. Sci. USA*, **101**, 423–428, doi:10.1073/pnas.2237157100.

Heidinger, A. K., M. J. Foster, A. Walther, and X. Zhao, 2014: The Pathfinder Atmospheres–Extended AVHRR climate dataset. *Bull. Amer. Meteor. Soc.*, **95**, 909–922, doi:10.1175/BAMS-D-12-00246.1.

Hutchison, K. D., R. L. Mahoney, E. F. Vermote, T. J. Kopp, J. M. Jackson, A. Sei, and B. D. Iisager, 2009: A geometry-based approach to identifying cloud shadows in the VIIRS cloud mask algorithm for NPOESS. *J. Atmos. Oceanic Technol.*, **26**, 1388–1397, doi:10.1175/2009JTECHA1198.1.

Jones, H. A., 1913: Effects of dust on the melting of snow. *Mon. Wea. Rev.*, **41**, 599, doi:10.1175/1520-0493(1913)41<599a:EODOTM>2.0.CO;2.

Marks, D., and J. Dozier, 1992: Climate and energy exchange at the snow surface in the alpine region of the Sierra Nevada: 2. Snow cover energy balance. *Water Resour. Res.*, **28**, 3043–3054, doi:10.1029/92WR01483.

——, J. Kimball, D. Tingey, and T. Link, 1998: The sensitivity of snowmelt processes to climate conditions and forest cover during rain-on-snow: A case study of the 1996 Pacific Northwest flood. *Hydrol. Processes*, **12**, 1569–1587, doi:10.1002/(SICI)1099-1085(199808/09)12:10/11<1569::AID-HYP682>3.0.CO;2-L.

Miller, S. D., A. P. Kuciauskas, M. Liu, Q. Ji, J. S. Reid, D. W. Breed, A. L. Walker, and A. A. Mandoos, 2008: Haboob dust storms of the southern Arabian Peninsula. *J. Geophys. Res.*, **113**, D01202, doi:10.1029/2007JD008550.

Neff, J. C., and Coauthors, 2008: Increasing eolian dust deposition in the western United States linked to human activity. *Nat. Geosci.*, **1**, 189–195, doi:10.1038/ngeo133.

Painter, T. H., A. P. Barrett, C. C. Landry, J. C. Neff, M. P. Cassidy, C. R. Lawrence, K. E. McBride, and G. L. Farmer, 2007: Impact of disturbed desert soils on duration of mountain snow cover. *Geophys. Res. Lett.*, **34**, L12502, doi:10.1029/2007GL030284.

——, J. S. Deems, J. Belnap, A. F. Hamlet, C. C. Landry, and B. Udall, 2010: Response of Colorado River runoff to dust radiative forcing in snow. *Proc. Natl. Acad. Sci. USA*, **107**, 17 125–17 130, doi:10.1073/pnas.0913139107.

——, A. C. Bryant, and S. M. Skiles, 2012a: Radiative forcing by light absorbing impurities in snow from MODIS surface reflectance data. *Geophys. Res. Lett.*, **39**, L17502, doi:10.1029/2012GL052457.

——, S. M. Skiles, J. S. Deems, A. C. Bryant, and C. C. Landry, 2012b: Dust radiative forcing in snow of the upper Colorado River basin: 1. A 6 year record of energy balance, radiation, and dust concentrations. *Water Resour. Res.*, **48**, W07521, doi:10.1029/2012WR011985.

——, F. C. Seidel, A. C. Bryant, S. M. Skiles, and K. Rittger, 2013: Imaging spectroscopy of albedo and radiative forcing by light-absorbing impurities in mountain snow. *J. Geophys. Res. Atmos.*, **118**, 9511–9523, doi:10.1002/jgrd.50520.

Pinker, R. T., and I. Laszlo, 1992: Modeling surface solar irradiance for satellite applications on a global scale. *J. Appl. Meteor.*, **31**, 194–211, doi:10.1175/1520-0450(1992)031<0194:MSSIFS>2.0.CO;2.

Prospero, J. M., 1999: Long-range transport of mineral dust in the global atmosphere: Impact of African dust on the environment of the southeastern United States. *Proc. Natl. Acad. Sci. USA*, **96**, 3396–3403, doi:10.1073/pnas.96.7.3396.

Ricchiazzi, P., S. R. Yang, C. Gautier, and D. Sowle, 1998: SBDART: A research and teaching software tool for plane-parallel radiative transfer in the earth's atmosphere. *Bull. Amer. Meteor. Soc.*, **79**, 2101–2114, doi:10.1175/1520-0477(1998)079<2101:SARATS>2.0.CO;2.

Salomonson, V. V., and I. Appel, 2004: Estimating fractional snow cover from MODIS using the normalized difference snow index. *Remote Sens. Environ.*, **89**, 351–360, doi:10.1016/j.rse.2003.10.016.

Schaepman-Strub, G., M. Schaepman, T. H. Painter, S. Dangel, and J. V. Martonchik, 2006: Reflectance quantities in optical remote sensing—Definitions and case studies. *Remote Sens. Environ.*, **103**, 27–42, doi:10.1016/j.rse.2006.03.002.

Schmit, T. J., M. M. Gunshor, W. P. Menzel, J. J. Gurka, J. Li, and A. S. Bachmeier, 2005: Introducing the next generation advanced baseline imager on GOES-R. *Bull. Amer. Meteor. Soc.*, **86**, 1079–1096, doi:10.1175/BAMS-86-8-1079.

Semmens, K. A., and J. Ramage, 2012: Investigating correlations between snowmelt and forest fires in a high-latitude snowmelt-dominated drainage basin. *Hydrol. Processes*, **26**, 2608–2617, doi:10.1002/hyp.9327.

Sengupta, M. A., A. Weekley, A. Habte, A. Lopez, C. Molling, and A. Heidinger, 2015: Validation of the National Solar Radiation Database (NSRDB) (2005-2012). Rep. NREL/CP-5D00-64981, 6 pp. [Available online at http://www.nrel.gov/docs/fy15osti/64981.pdf.]

Singh, S. K., A. V. Kulkarni, and B. S. Chaudhary, 2010: Hyperspectral analysis of snow reflectance to understand the effects of contamination and grain size. *Ann. Glaciol.*, **51**, 83–88, doi:10.3189/172756410791386535.

Skiles, S. M., 2014: Dust and black carbon radiative forcing controls on snowmelt in the Colorado River basin. Ph.D. thesis, University of California, Los Angeles, 274 pp. [Available online at http://escholarship.org/uc/item/27s9r0j9.]

——, T. H. Painter, J. S. Deems, A. C. Bryant, and C. C. Landry, 2012: Dust radiative forcing in snow of the upper Colorado River basin: 2. Interannual variability in radiative forcing and snowmelt rates. *Water Resour. Res.*, **48**, W07522, doi:10.1029/2012WR011986.

Stamnes, K., S.-C. Tsay, W. Wiscombe, and K. Jayaweera, 1988: Numerically stable algorithm for discrete-ordinate-method radiative transfer in multiple scattering and emitting layered media. *Appl. Opt.*, **27**, 2502–2509, doi:10.1364/AO.27.002502.

Steltzer, H., C. Landry, T. H. Painter, J. Anderson, and E. Ayres, 2009: Biological consequences of earlier snowmelt from desert dust deposition in alpine landscapes. *Proc. Natl. Acad. Sci. USA*, **106**, 11 629–11 634, doi:10.1073/pnas.0900758106.

Stowe, L. L., P. A. Davis, and E. P. McClain, 1999: Scientific basis and initial evaluation of the CLAVR-1 global clear/cloud classification algorithm for the Advanced Very High Resolution Radiometer. *J. Atmos. Oceanic Technol.*, **16**, 656–681, doi:10.1175/1520-0426(1999)016<0656:SBAIEO>2.0.CO;2.

Wake, C. P., and P. A. Mayewski, 1994: Modern eolian dust deposition in central Asia. *Tellus*, **46B**, 220–233.

Walther, A., and A. K. Heidinger, 2012: Implementation of the daytime cloud optical and microphysical properties algorithm (DCOMP) in PATMOS-x. *J. Appl. Meteor. Climatol*, **51**, 1371–1390, doi:10.1175/JAMC-D-11-0108.1.

Warren, S. G., and W. J. Wiscombe, 1980: A model for the spectral albedo of snow. II: Snow containing atmospheric aerosols. *J. Atmos. Sci.*, **37**, 2734–2745, doi:10.1175/1520-0469(1980)037<2734:AMFTSA>2.0.CO;2.

Westerling, A. L., H. G. Hidalgo, D. R. Cayan, and T. W. Swetnam, 2006: Warming and earlier spring increase western U.S. forest wildfire activity. *Science*, **313**, 940–943, doi:10.1126/science.1128834.

Weygandt, S., T. Smirnova, S. Benjamin, K. Brundage, S. Sahm, C. Alexander, and B. Schwartz, 2009: The High Resolution Rapid Refresh (HRRR): An hourly updated convection resolving model utilizing radar reflectivity assimilation from the RUC/RR. *23rd Conf. on Weather Analysis and Forecasting/19th Conf. on Numerical Weather Prediction*, Omaha, NE, Amer. Meteor. Soc., 15A.6. [Available online at https://ams.confex.com/ams/23WAF19NWP/webprogram/Paper154317.html.]

Wiscombe, W. J., and S. G. Warren, 1980: A model for the spectral albedo of snow. I: Pure snow. *J. Atmos. Sci.*, **37**, 2712–2733, doi:10.1175/1520-0469(1980)037<2712:AMFTSA>2.0.CO;2.

Zhu, Z., and C. E. Woodcock, 2014: Automated cloud, cloud shadow, and snow detection in multitemporal Landsat data: An algorithm designed specifically for monitoring land cover change. *Remote Sens. Environ.*, **152**, 217–234, doi:10.1016/j.rse.2014.06.012.